

Near-Real-Time analysis of the ionospheric response to the 15 January 2022 Hunga Tonga-Hunga Ha’apai volcanic eruption

Boris Maletckii¹, Elvira Astafyeva^{1,1}, and Boris Maletckii¹

¹Institut de Physique du Globe de Paris

December 1, 2022

Abstract

We present a near-real-time (NRT) scenario of analysis of ionospheric response to the 15 January 2022 Hunga Tonga-Hunga Ha’apai eruption by using GNSS data. We introduce a new method to determine instantaneous velocities using an interferometric approach and using the time derivative of the total electron content (TEC). Moreover, for the first time, we propose a novel method that automatically estimates the propagation velocity of disturbances from near-real-time travel-time diagrams. By using our new methods, we analyzed the dynamics of co-volcanic ionospheric disturbances generated by the Hunga-Tonga eruption, and we estimated the first propagation velocity to be ~ 800 - 950 m/s, which subsequently decreased to ~ 600 m/s. We demonstrate that our approach can be used to detect, analyze and identify the complexity of a natural hazard event. Also, it is important to note that our new methods can perform at a low spatial resolution and 30-sec cadence data.

1 **Near-Real-Time analysis of the ionospheric response to the 15 January 2022 Hunga**
2 **Tonga-Hunga Ha'apai volcanic eruption**
3

4 **B. Maletckii¹ and E. Astafyeva¹**

5 ¹ Université Paris Cité, Institut de Physique du Globe de Paris (IPGP), CNRS UMR 7154, 35-39
6 Rue Hélène Brion, 75013 Paris, email : maletckii@ipgp.fr

7 Corresponding author: Boris Maletckii (maletckii@ipgp.fr)
8

9 **Key Points:**

- 10 • We suggest novel methods that detect and characterize ionospheric disturbances due to
11 the Tonga Eruption in the Near-Real-Time (NRT)
- 12 • In NRT total electron content time derivative (dTEC/dt), we observe multiple response
13 signatures that indicate multiple eruption scenario
- 14 • The peak-to-peak amplitude of the dTEC/dt is comparable to the 2011 Tohoku-Oki
15 earthquake and the 28 October 2003 solar flare
16

17 **Abstract**

18 We present a near-real-time (NRT) scenario of analysis of ionospheric response to the 15
19 January 2022 Hunga Tonga-Hunga Ha’apai eruption by using GNSS data. We introduce a new
20 method to determine instantaneous velocities using an interferometric approach and using the
21 time derivative of the total electron content (TEC). Moreover, for the first time, we propose a
22 novel method that automatically estimates the propagation velocity of disturbances from near-
23 real-time travel-time diagrams. By using our new methods, we analyzed the dynamics of co-
24 volcanic ionospheric disturbances generated by the Hunga-Tonga eruption, and we estimated the
25 first propagation velocity to be $\sim 800\text{-}950$ m/s, which subsequently decreased to ~ 600 m/s. We
26 demonstrate that our approach can be used to detect, analyze and identify the complexity of a
27 natural hazard event. Also, it is important to note that our new methods can perform at a low
28 spatial resolution and 30-sec cadence data.

29 **Plain Language Summary**

30 Volcanic eruptions are known to generate strong pressure perturbations that propagate up to the
31 upper atmosphere and generate disturbances in the atmosphere’s ionized part - the ionosphere.
32 The 15 January 2022 Hunga Tonga-Hunga Ha’apai submarine volcanic eruption created quite a
33 significant response in the ionosphere. By using a local network of Global Navigation Satellite
34 Systems (GNSS) receivers, we analyze ionospheric response in the near-field area of the
35 volcano. This information can help to complement conventional instruments, since they are not
36 available around the volcano. Therefore, it is important to perform an analysis in near-real-time
37 (NRT). To do so, we introduce novel automatic methods to characterize properties of the
38 response generated by the volcano only by ionospheric GNSS data. These methods suggest the
39 first velocities to be $\sim 800\text{-}900$ m/s, subsequently slowing down to ~ 600 m/s. Besides, our
40 approach allowed us to observe a multi-eruptional scenario.

41 **1 Introduction**

42 It is known that natural hazards, such as earthquakes, tsunamis, and volcanic eruptions
43 generate acoustic and gravity waves that propagate upward in the atmosphere and ionosphere
44 (Astafyeva, 2019). Ionospheric disturbances generated by volcanic eruptions are called co-
45 volcanic ionospheric disturbances (co-VID). It is known that the co-VID are usually quasi-
46 periodically shaped variations that occur ~ 10 to 45 min after the eruption onset, last for 1-1.5
47 hours, occur in the near field of a volcano (up to ~ 2000 km), with velocities in the range of 0.5
48 km/s - 1.1 km/s (Heki, 2006; Dautermann et al., 2009; Nakashima et al., 2016; Liu et al., 2017).

49 Nowadays, we can detect the co-VID by ground-based GNSS receivers. Going further
50 forward, Shults et al. (2016) introduced for the first time a term “Ionospheric Volcanology” that
51 refers to the use of ionospheric measurements for the interests of volcanology. For instance, from
52 the co-VID measurements, it is possible to determine the location of an eruptive volcano, the
53 time of eruption onset (Shults et al., 2016), and estimate volcanic eruption power (Heki, 2006;
54 Dautermann et al., 2009; Manta et al., 2021). Ionospheric-based methods would complement

55 conventional ones, which use data from nearby seismometers and infrasound stations. The
 56 accuracy of those conventional methods decreases in absence of instrumentation within ~100 km
 57 from a volcano. To make a step forward toward ionospheric volcano monitoring and warning
 58 systems we must develop real or near-real-time (NRT) methods.

59
 60 In this work, we analyze ionospheric disturbances caused by the 15 January 2022 massive
 61 eruption of Hunga Tonga-Hunga Ha’apai (HTHH) volcano. Since the volcano is a submarine
 62 one, there are no ground-based instruments nearby, which makes it difficult to calculate the onset
 63 time of the eruption. For instance, the US Geological Survey (USGS),
 64 <https://earthquake.usgs.gov/earthquakes/eventpage/pt22015050/executive>) estimated the onset at
 65 04:14:45 UT, Poli and Shapiro (2022) - at 04:16:00 UT, while satellite data suggest the onset
 66 between 04:00 and 04:10 UT. Unreachability of conventional tools makes this eruption a perfect
 67 example of when the "Ionospheric Volcanology" could contribute to the. Here, for the first time,
 68 we present an NRT scenario of spatio-temporal analysis for this eruption. In addition, also for the
 69 first time, we present a new method to determine the co-VID velocity from near-real-time travel-
 70 time diagrams (NRT TTD).

71 2 Data and Methods

72 Global Navigation Satellite Systems (GNSS) are a helpful tool for ionospheric sounding.
 73 Its main advantage is good spatial and temporal resolution. Phase measurements from dual-
 74 frequency GNSS receivers allow estimation of the ionospheric total electron content (TEC),
 75 which is equal to the number of electrons along a line-of-sight (LOS) between a satellite and a
 76 receiver:

$$77$$

$$78 \quad TEC_{ij} (phase, slant) = \frac{1}{A} \times \frac{f_i^2 f_j^2}{f_i^2 - f_j^2} \times (L_i \lambda_i - L_j \lambda_j) \quad (1)$$

79
 80 where $A = 40.308 \text{ m}^3/\text{s}^2$, L_i and L_j are phase measurements, λ_i and λ_j are wavelengths at the two
 81 the given frequencies (for Global Positioning System (GPS) $i=1, j=2$ and frequencies are 1575.42
 82 and 1227.60 MHz, respectively). The TEC is measured in TEC units (TECu), $1 \text{ TECu} = 10^{16}$
 83 electrons/ m^2 .

84 We use the ionospheric thin shell approximation to calculate the spatial positions of
 85 ionospheric disturbances. The intersection points between the LOS and this shell (at a fixed
 86 altitude H_{ion}) are ionospheric pierced points (IPP). We use $H_{\text{ion}} = 320 \text{ km}$ since it is close to the
 87 maximum ionization height H_mF2 (based on the nearest ionosonde station NIUE at 169.9E;
 88 19.1S).

89 To study the co-VID signatures driven by the HHTH volcano eruption, we analyze data
 90 of 24 ground-based GNSS-receivers in the near-field, i.e., under ~2000 km away from the
 91 volcano. To extract the co-VID signatures from the TEC data series, researchers usually apply 1-
 92 4 mHz band-pass filters (Heki, 2006; Shults et al., 2016; Nakashima et al., 2016; Manta et al.,

93 2021). However, in a real-time scenario it is not possible because of the following reasons: a) the
94 impossibility to stack long series of data in NRT; b) such signal properties as arrival time,
95 amplitude, and spectral components can be affected by the filter parameters (Maletckii et al.,
96 2020). For NRT, we propose to use the TEC time derivative, which works as a high-pass filter
97 and removes the bias and trend caused by the satellite orbit motion. In addition, our $d\text{TEC}/dt$
98 approach will not modify the amplitude of the co-VID.

99 By using the TEC time derivative approach, Maletckii and Astafyeva (2021a) introduced
100 a method “D1-GNSS-RT” allowing to calculate spatio-temporal properties of traveling
101 ionospheric disturbances (TID) in NRT (Figure 1). To detect TID, the “D1-GNSS-RT” method
102 first analyses TEC data series to find the local maximum value (LMV). Then, it computes the
103 cross-correlation function for each pair of time series around the LMV to calculate the difference
104 in TID arrivals. Finally, based on these time shifts and by using an interferometric approach it
105 estimates the horizontal velocities of TID propagation. The “D1-GNSS-RT” method was tested
106 on several earthquakes but only showed good results with 1-sec data and on dense GNSS
107 networks, such as Japan GEONET. The latter restrictions make it challenging to apply this
108 method to the analysis of the co-VID generated by the HHTH volcanic eruption. The spatial
109 coverage around the Tonga Islands is rather sparse, and only 16 out of 24 GNSS stations provide
110 both 1-sec and 30-sec cadence data, while the others are limited to only 30-sec cadence data
111 (Figure 2a). Besides, 30-sec $d\text{TEC}/dt$ signals have smaller amplitudes and narrower spectral
112 composition, which results in less pronounced signals as compared to 1-sec $d\text{TEC}/dt$ data (Figure
113 S1).

114 Here, for the first time, we introduce a new “D1-GNSS-RT” applicable to 30-sec data.
115 The main developments are presented in Figure 1. They include: 1) increase of the LMV window
116 to 7 minutes, 2) increase of the cross-correlation window to 24 minutes; 3) decrease of the
117 threshold of the coefficient of the cross-correlation function down to 0.7. However,
118 unfortunately, these new parameters modify the definition of NRT from 15 minutes for 1-sec
119 data to 30 minutes for 30-sec data.

120 When the “D1-GNSS-RT” is not applicable (e.g., sparse GNSS coverage), the horizontal
121 TID velocity can be estimated by using travel-time diagrams, or hodocrones, that present the
122 TEC variations with respect to the source location and time. Similar to the D1-GNSS-RT, for
123 NRT-TTD we also use the $d\text{TEC}/dt$ parameter. As the source, we take the volcano position.
124 From TTD, the velocity can be estimated as the slope, however, up to now, there was no NRT-
125 compatible automatic method to do that. Here, for the first time, we developed a novel
126 technique to fit the slope line in NRT.

127 The automatic NRT TTD fitting technique consists of two stages: 1) the first maximum
128 “picker” and 2) the “fitter” based on these maxima.

129 To select the maximum along with all $d\text{TEC}/dt$ values, we pick the values exceeding a standard
130 deviation of the series and a threshold of 0.15 TECu. In the case of the multiple values in the
131 120-second windows, we chose the centered one in this window. We also remove outliers from

132 the final list of maxima in the given series (values that can appear only with velocities exceeding
133 5 km/s).

134 We use the first maximum of each data series to fit the first velocity slope. They are
135 sorted based on the source distance - from the closest to the farthest. By analyzing the velocity
136 between the current and previous maximum point we decide whether this maximum is
137 “physically” suitable for the fitting process (velocity between two points should be in the range
138 between 0.1 and 5 km/s and should not vary for more than 20% with respect to the velocity
139 between two previous points; after picking the first 8 suitable maxima we add a new condition -
140 the velocity should not change for more than 50% of the average velocity of all previous points).
141 After the list of suitable points is finished, we fit the slope line by linear regression in these
142 points.

143 In the case of the Quasi-NRT method, we added a second round for the picking process.
144 After we obtain the first NRT velocity we compare all first maximum velocities with this value.
145 If it lies in a 20% difference border interval, we pick this maximum. The new list of points is
146 used for the Quasi-NRT fitting.

147 Since the second round would require more time, we call this method “Quasi-NRT”.
148 However, the Quasi-NRT method seems to be more accurate, therefore it can be used to
149 determine NRT-method accuracy in a particular case.

150 **3 Results and Discussion**

151 As shown recently, the explosive eruption of HTHH volcano produced quite a significant
152 response in the ionosphere, and eruption-driven traveling ionospheric disturbances (TID) were
153 observed as far as 20,000 km away from the volcano (Themens et al., 2022; Zhang et. al., 2022).
154 The amplitude of the near-field response reached as high value as 5-8 TECu (Astafyeva E. et. al.,
155 2022). In the case of the dTEC/dt parameter, we observe a peak-to-peak disturbance amplitude of
156 ~8 TECu, which is extraordinary (Figure S2). This value exceeds by a factor of 2.5-3 all
157 previously recorded co-VID (Figure S2). Such large amplitudes were only observed during the
158 2011 Tohoku-Oki earthquake and during the 28th October 2003 solar flare (Figure S2).

159 To analyze HTHH-driven response in the NRT scenario, we use our newly developed
160 methods. We estimate spatio-temporal evolution of co-VID, including the amplitude of the
161 velocity, the azimuths of propagation, and the ionospheric source location.

162

163 **3.1 Spatio-temporal characteristics of the co-VID from D1-GNSS-RT. The** 164 **instantaneous velocities’ field and source location.**

165 The co-VID velocity field maps for the first arrivals following the Hunga-Tonga eruption are
166 shown in Fig. 2b–d, and the localization results are presented in Fig. 2e–f. Figure 2b shows the
167 first velocity vectors at 04:23:30 UT, i.e., 525s after the eruption onset time, both on the north-
168 east and south-west out from the volcano. From the time of the first co-VID detection, in the
169 NRT scenario, we need 22 minutes more to compute the first velocity field, which is an increase
170 of the time delay for the NRT method as compared to 1-sec data. The two main reasons are a

171 long 30-sec cross-correlation window (24 minutes vs. 5 minutes with 1-sec data) and sparse
172 spatial resolution. The latter signifies fewer IPP that can be selected for correlation triangles after
173 the first co-VID detection. Therefore, more time is necessary to “form” an interferometric
174 triangle. The first vectors propagate in directions outward from the source. The first horizontal
175 velocities of the co-VID are about $\sim 830\text{-}900$ m/s, i.e., they correspond to acoustic and shock-
176 acoustic waves, and are in line with retrospective studies (e.g., Themens et al., 2022). The first
177 velocity vectors are used to compute the first source location at the point with coordinates
178 (17.90S; 176.26E) (Fig. 2e). The subsequent co-VID evolution during the next 2 minutes
179 maintains the tendency for both the outward direction of propagation and velocities’ values.
180 Further, the velocities decrease to $\sim 500\text{-}600$ m/s, while the source locations concentrate
181 northwest of the volcano (Fig. 2f).

182

183 **3.2 Spatio-temporal characteristics of the co-VID from NRT TTD using 30-sec data.**

184 The 30-sec NRT-TTD for all satellites and receivers (e.g, all LOS) is shown in Figure 3.
185 From these data, our newly developed method estimates the velocity to be 621.1 km/s. This value
186 is in line with previous retrospective observations for the ionospheric response to the Hunga-
187 Tonga eruption (Themens et al., 2022), as well as with our “D1-GNSS-RT” results. The error of
188 the velocity estimations is less than 10% for both NRT and Quasi-NRT method (Figure 4). The
189 difference between NRT and Quasi-NRT estimations is 11,1%. We can observe the existence of
190 the co-VID signatures before the fitted slope line on Figure 3, but the amplitudes of the
191 disturbances were not sufficient for the “picker” part of the automatic NRT TTD fitting
192 technique.

193

194

195 **3.3 Spatio-temporal characteristics of the co-VID from NRT TTD using 1-sec data.**

196 As mentioned above, only 16 GNSS receivers in the near-field of the HTHH volcano
197 provided 1-sec data. This number is too few to use the 1-sec “D1-GNSS-RT” method. However,
198 these limits do not apply to NRT TTD. Figure 5 shows the dTEC/dt-based TTD plotted for co-
199 VID observed in the near-field. We note that the high-rate response to the HTHH volcanic
200 eruption is more complex than the 30-sec one. Figure 5b demonstrates the occurrence of four
201 dTEC/dt disturbances that are, most likely, related to four independent eruptive events that
202 occurred between 04:00 and 05:30 UT. The separate events can be distinguished on TTD based
203 on the characteristics of the ionospheric responses, such as signal shape, the apparent velocity of
204 propagation, and the amplitude.

205 The NRT TTD shows one quasi-periodic and three N-shaped signatures (dotted ovals in
206 Figure 5b). The first quasi-periodic response (in the green circle) has the lowest velocity along
207 with the others (~ 0.5 km/s). For the second response the slope gives the apparent velocity of
208 ~ 1.33 km/s. It appears to consist of three N-shaped signals which have identical velocity slopes.
209 Further, we distinguish the third event based on a new increase in the dTEC/dt from $\sim 05:15$ UT.

210 For this component, the velocity slope is ~ 2 km/s. Finally, the fourth event has an apparent
211 velocity of ~ 1.33 km/s, which distinguishes it from the third event, although it is close in time.

212 Figure 5a shows an example of $d\text{TEC}/dt$ signatures for SAMO-R21 (in blue-white-red
213 colormap). We also implement a centered moving average filter (5-sec window) to this series
214 (black curve), which allow to remove noise in data and to concentrate mostly on useful
215 variations. The results prove an assumption of two types of the signatures: first, quasi-periodic
216 and then, N-shaped ones. Evenmore, we observed the first co-VID driven signatures a couple of
217 minutes before USGS determined eruption onset time. Generally, it would need ~ 7 -10 minutes
218 for disturbances to reach the ionospheric altitudes, therefore the eruption onset occurred between
219 04:00 and 04:10.

220 Since we observe a difference in the eruption onset time between our results and on-
221 ground techniques, we estimate it based on the slopes and the TTD (Figure 5c). To do so, we
222 first compute the intersection of the velocity slope line with the 0-km distance from the source.
223 Second, we estimate the time in the intersection point from the TTD. This time corresponds to
224 the onset time in the ionosphere, which is the time when the eruption-driven acoustic wave
225 reaches the ionosphere (i.e., the altitude of detection, $H_{\text{ion}} = 320$ km). Third, we compute the
226 vertical propagation time for the acoustic wave from the volcano to the ionosphere by using the
227 sound speed profile derived from the NRLMSISE-2 model (Emmert et al., 2020). With a
228 weighted average velocity of the sound speed of 470 m/s (Figure S3b), the acoustic wave will
229 take ~ 11.34 minutes (11 minutes 20 seconds) to reach 320 km of altitude. Finally, we extract this
230 propagation time from the ionospheric onset times in order to obtain the ground onset times for
231 all four events (Table S1). From our method it follows that the HTHH volcano began to erupt at
232 04:08:26 UT, which is in agreement with satellite observations that suggest the eruption onset
233 between 04:00 and 04:10 UT (Gusman and Rodger, 2022). Our onset time is also very close to
234 that estimated by Astafyeva et al. (2022) from raw unfiltered TEC data by retrospective analysis.
235 However, it is several minutes earlier than seismically-determined onset time (USGS; Poli &
236 Shapiro, 2022), and ~ 20 minutes earlier than the onset estimated by using a pressure station at
237 Tonga (Wright et al, 2022). Our work demonstrates that our ionosphere-based NRT approach
238 can be successfully used along with conventional methods.

239 The occurrence of multiple eruptive events, that is clearly seen in $d\text{TEC}/dt$ data, is in line
240 with previous reports. For instance, Wright et al. (2022) identified four independent events that
241 occurred between 04:00 and 05:30 UT: 04:26 UT, 04:36 UT, 05:10 UT, 05:51 UT. Astafyeva et
242 al, 2022 suggested the occurrence of five eruptive events between 04:00 and 05:30 UT, however
243 their onset times differ from our estimations since the approximations are different.

244 **4 Conclusions**

245 In this work, we performed for the first time a near-real-time analysis of the ionospheric response
246 to the massive 15 January 2022 Hunga Tonga-Hunga Ha'apai explosive eruption. Our main
247 developments and findings are summarized below:

- 248 1. For the first time, we introduce a new method to determine spatio-temporal characteristics in
249 the NRT. This method estimates the instantaneous velocities and the ionospheric source
250 location using not only high-rate data but also the “standard” 30-sec data. In addition, our
251 new method can perform in sparse spatial coverage conditions. We note, however, that 30-
252 sec data increase the NRT time delay between the event onset and the first results to ~30
253 minutes. By using this method, in a near-real-time scenario applied for the HTHH eruption
254 case, we estimate the first instantaneous velocities to be ~800-900 m/s, which is in line with
255 retrospective studies (e.g., Themens et al., 2022; Zhang et al., 2022), and correspond to
256 acoustic and shock-acoustic waves. The location of the ionospheric source determined by
257 our method is in the northwest of the volcano.
- 258 2. For the first time, we present a new method that can estimate the co-VID velocity by using a
259 real-time travel-time diagram. For the HTHH volcanic eruption, we observe the apparent co-
260 VID propagation speed to be 621.1 m/s. This value is in line with our “D1-GNSS-RT”
261 results.
- 262 3. Our dTEC/dt NRT-TTD suggest the occurrence of four distinct eruptions between 04:00 and
263 05:30 UT. From the velocity slopes in NRT-TTD, we estimate the onset time for the four
264 events at 04:08:43 UT, 04:31:00 UT, 05:02:30 UT, and 05:05:21 UT. The multi-eruption
265 scenario is an agreement with the analysis of surface pressure data (Wright et al., 2022) and
266 that of the unfiltered ionosphere TEC data (Astafyeva et al., 2022).
- 267 4. We emphasize that the amplitude of the dTEC/dt ionospheric response to the HTHH
268 volcanic eruption is unprecedentedly strong as compared to previously recorded dTEC/dt
269 disturbances. The peak-to-peak dTEC/dt disturbance amplitude exceeded by a factor of 2.5-
270 3 all previously recorded co-VID. According to our knowledge, only two events produced
271 dTEC/dt response with similar magnitude: the 2011 Great Tohoku-Oki earthquake and the
272 28 October 2003 solar flare.

273

274 Our results once again demonstrate the advantages of the use of the dTEC/dt parameter as the
275 effective NRT tool to rapidly determine dynamic characteristics of ionospheric disturbances. We
276 also demonstrate that an ionosphere-based method can be a reliable alternative for detection of
277 natural hazard events. This is especially important and useful for the analysis of submarine
278 events, such as the HTHH volcanic eruption, where ground-based instrumentation is lacking.

279 Acknowledgments

280 We thank the French Space Agency (CNES, Project “RealDetect”) for the support. BM
281 additionally thanks the CNES and the IPGP for the Ph.D. fellowship. We acknowledge the use of
282 “tec-suite” codes developed by I. Zhivetiev (<https://tec-suite.readthedocs.io/en/latest/>).

283 The authors thank Rolland L., Coisson P., Mikesell T. D., Ravanelli M., Munaibari E. and Manta
284 F. for valuable discussion.

285

286 Open Research

287 All GNSS data are available from the CDDIS data archives
 288 (<https://cddis.nasa.gov/archive/gnss/data/daily/>).

289 Ionosonde station NIUE data are available from the DIDBase Web Portal
 290 ([https://lgdc.uml.edu/common/DIDBMonthListForYearAndStation?ursiCode=ND61R&year=20](https://lgdc.uml.edu/common/DIDBMonthListForYearAndStation?ursiCode=ND61R&year=2022)
 291 [22](https://lgdc.uml.edu/common/DIDBMonthListForYearAndStation?ursiCode=ND61R&year=2022)).

292 Figures were plotted by using Python (ver. 3.7, libraries “matplotlib.pyplot”:
 293 https://matplotlib.org/3.5.0/api/as_gen/matplotlib.pyplot.html and “cartopy”:
 294 <https://scitools.org.uk/cartopy/docs/latest/>)
 295

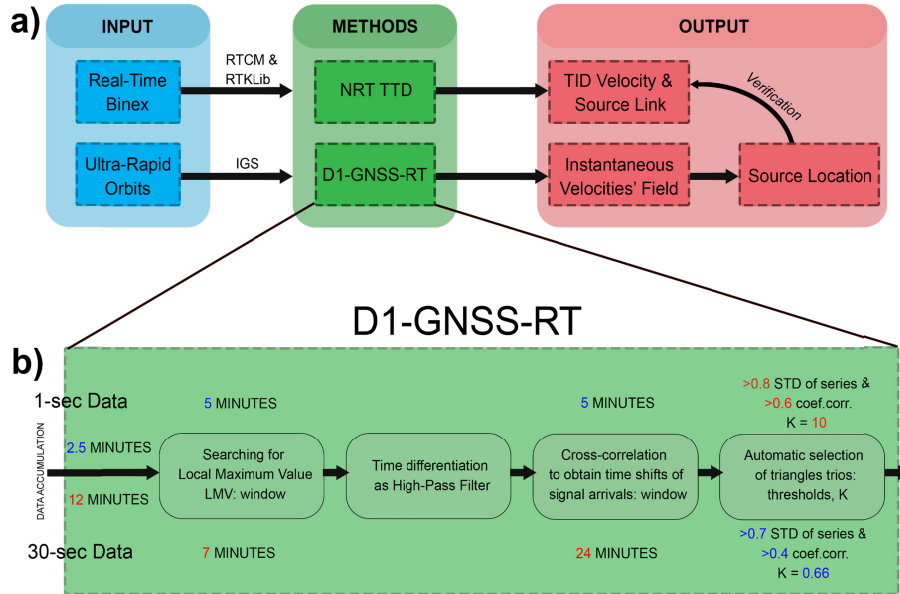
296 References

- 297 1. Astafyeva, E. (2019) Ionospheric detection of natural hazards. *Reviews of Geophysics*
 298 57(4), 1265-1288. [doi.org: 10.1029/2019RG000668](https://doi.org/10.1029/2019RG000668)
- 299 2. Astafyeva, E., Maletckii, B., Mikesell, T. D., Munaibari, E., Ravanelli, M., Coisson, P., et
 300 al. (2022). The 15 January 2022 Hunga Tonga eruption history as inferred from
 301 ionospheric observations. *Geophysical Research Letters*, 49, e2022GL098827.
 302 doi.org/10.1029/2022GL098827
- 303 3. Dautermann, T., Calais, E., & Mattioli, G. S. (2009). Global Positioning System detection
 304 and energy estimation of the ionospheric wave caused by the 13 July 2003 explosion of
 305 the Soufrière Hills Volcano, Montserrat. *Journal of Geophysical Research*, 114(B2),
 306 B02202. [doi.org: 10.1029/2008JB005722](https://doi.org/10.1029/2008JB005722)
- 307 4. Emmert, J. T., Drob, D. P., Picone, J. M., Siskind, D. E., Jones, M., Mlynczak, M. G., et
 308 al. (2020). NRLMSISE 2.0: A whole-atmosphere empirical model of temperature and
 309 neutral species densities. *Earth and Space Science*, 8, e2020EA001321.
 310 <https://doi.org/10.1029/2020EA001321>
- 311 5. Gusman, A.R. & Roger, J. (2022). Hunga Tonga - Hunga Ha’apai volcano-induced sea
 312 level oscillations and tsunami simulations. GNS Science webpage, [doi.org:](https://doi.org/10.21420/DYKJ-RK41)
 313 [10.21420/DYKJ-RK41](https://doi.org/10.21420/DYKJ-RK41)
- 314 6. Heki, K. (2006) Explosion energy of the 2004 eruption of the Asama Volcano, central
 315 Japan, inferred from ionospheric disturbances, *Geophys. Res. Lett.*, 33, L14303, [doi:](https://doi.org/10.1029/2006GL026249)
 316 [10.1029/2006GL026249](https://doi.org/10.1029/2006GL026249).
- 317 7. Liu, X., Zhang, Q., Shah, M., & Hong, Z. (2017). Atmospheric-ionospheric disturbances
 318 following the April 2015 Calbuco volcano from GPS and OMI observations. *Advances in*
 319 *Space Research*, 60 (12), 2836–2846. [doi.org: 10.1016/j.asr.2017.07.007](https://doi.org/10.1016/j.asr.2017.07.007)
- 320 8. Maletckii, B., Yasyukevich, Y., & Vesnin, A. (2020). Wave Signatures in Total Electron
 321 Content Variations: Filtering Problems. *Remote Sensing*, 12(8), 1340. [doi.org:](https://doi.org/10.3390/rs12081340)
 322 [10.3390/rs12081340](https://doi.org/10.3390/rs12081340)
- 323 9. Maletckii, B. and Astafyeva, E. (2021a) Determining spatio-temporal characteristics of
 324 Coseismic Travelling Ionospheric Disturbances (CTID) in near real-time. *Scientific*
 325 *Reports*, 11:20783, [doi: 10.1038/s41598-021-99906-5](https://doi.org/10.1038/s41598-021-99906-5).
- 326 10. Maletckii, B. and Astafyeva, E. (2021b) Near-Real-Time Analysis of Spatio-Temporal
 327 Characteristics of Ionospheric Disturbances of Different Origins. *Session SA022, AGU*
 328 *Fall Meeting 2021, 13-17 December 2021, Hybrid, New Orleans, USA*
- 329 11. Manta, F., G. Occhipinti, E. Hill, A. Perttu, B. Taisne (2021) Correlation Between
 330 GNSS-TEC and Eruption Magnitude Supports the Use of Ionospheric Sensing to

- 331 Complement Volcanic Hazard Assessment, J. Geophys. Res. - Solid Earth, [doi:](https://doi.org/10.1029/2020JB020726)
332 [10.1029/2020JB020726](https://doi.org/10.1029/2020JB020726)
- 333 12. Nakashima, Y., Heki, K., Takeo, A., Cahyadi, M. N., Aditiya, A., & Yoshizawa, K.
334 (2016). Atmospheric resonant oscillations by the 2014 eruption of the Kelud volcano,
335 Indonesia, observed with the ionospheric total electron contents and seismic signals.
336 Earth and Planetary Science Letters, 434, 112–116. [doi.org: 10.1016/j.epsl.2015.11.029](https://doi.org/10.1016/j.epsl.2015.11.029)
- 337 13. Noll, C. E. & System, T. C. D. D. I. (2010) A resource to support scientific analysis using
338 space geodesy. Adv. Space Res. 45(12), 1421–1440. [doi.org: 10.1016/j.asr.2010.01.018](https://doi.org/10.1016/j.asr.2010.01.018) .
- 339 14. Poli, P. and M. Shapiro (2022) Rapid characterization of large volcanic eruptions:
340 measuring the impulse of the Hunga Tonga explosion from teleseismic waves. ESSOAr,
341 [doi.org: 10.1002/essoar.10510358.1](https://doi.org/10.1002/essoar.10510358.1)
- 342 15. RTCM. (2020) Radio Technical Commission for Maritime Services.
343 <https://www.rtcn.org/>
- 344 16. Shults, K., E. Astafyeva and S. Adourian (2016). Ionospheric detection and localization
345 of volcano eruptions on the example of the April 2015 Calbuco events. J. Geophys. Res. -
346 Space Physics, V.121, N10, 10,303-10,315, [doi.org: 10.1002/2016JA023382](https://doi.org/10.1002/2016JA023382).
- 347 17. Themens, D. R., Watson, C., Žagar, N., Vasylyevych, S., Elvidge, S., McCaffrey, A., et
348 al. (2022). Global propagation of ionospheric disturbances associated with the 2022
349 Tonga Volcanic Eruption. *Geophysical Research Letters*, 49, e2022GL098158. [doi.org:](https://doi.org/10.1029/2022GL098158)
350 [10.1029/2022GL098158](https://doi.org/10.1029/2022GL098158)
- 351 18. Takasu, T. (2013) RTKLIB: An Open Source Program Package for GNSS Positioning.
352 <http://www.rtklib.com>
- 353 19. Wright, C.J., et al. (2022) Tonga eruption triggered waves propagating globally from
354 surface to edge of space, *ESSOAr*,
355 <https://www.essoar.org/pdfjs/10.1002/essoar.10510674.1>
- 356 20. Zhang, S.-R., et al. (2022) 2022 Tonga Volcanic Eruption Induced Global Propagation of
357 Ionospheric Disturbances via Lamb Waves. *Frontiers in Astronomy and Space Sciences*,
358 8, [doi.org: 10.3389/fspas.2022.871275](https://doi.org/10.3389/fspas.2022.871275)

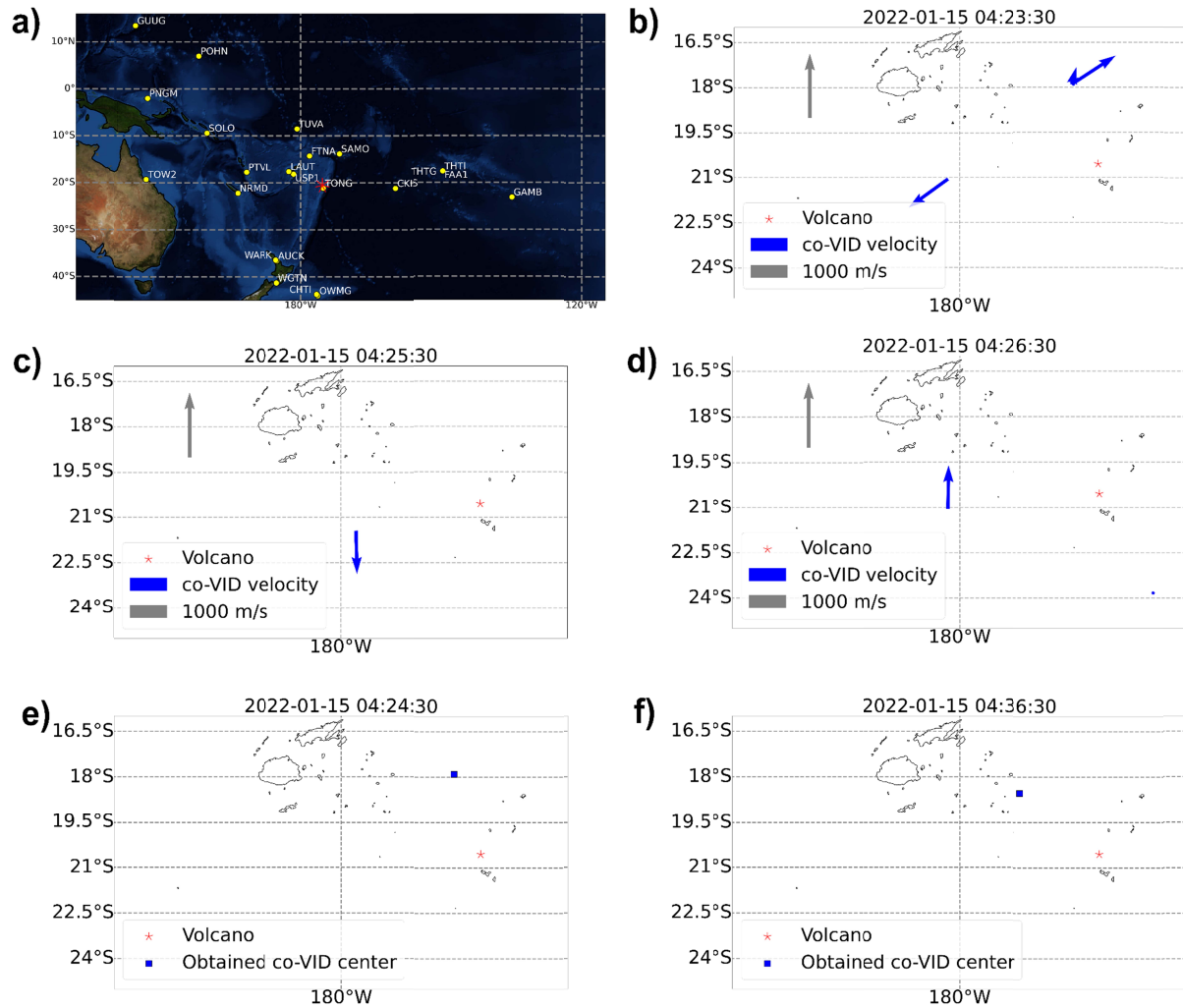
360 **Figures Captions**

361 **Figure 1.** Scheme of methods developed and implemented in this work. “D1-GNSS-RT” and
 362 NRT TTD methods require Real-Time TEC (can be transferred by RTKlib software (Takasu,
 363 2013) and RTCM protocol (RTCM, 2020)) and orbits (can be obtained by Ultra-Rapid Orbits
 364 provided by IGS (Noll, 2010)) data. “D1-GNSS-RT” method provides the instantaneous
 365 velocities’ field. Based on it, we compute the source location. NRT TTD estimates TID velocity
 366 and verifies the link with the source location. The upper part shows the difference in method
 367 parameters between the 1-sec “D1-GNSS-RT” and 30-sec “D1-GNSS-RT” that was developed
 368 and implemented here for the first time.



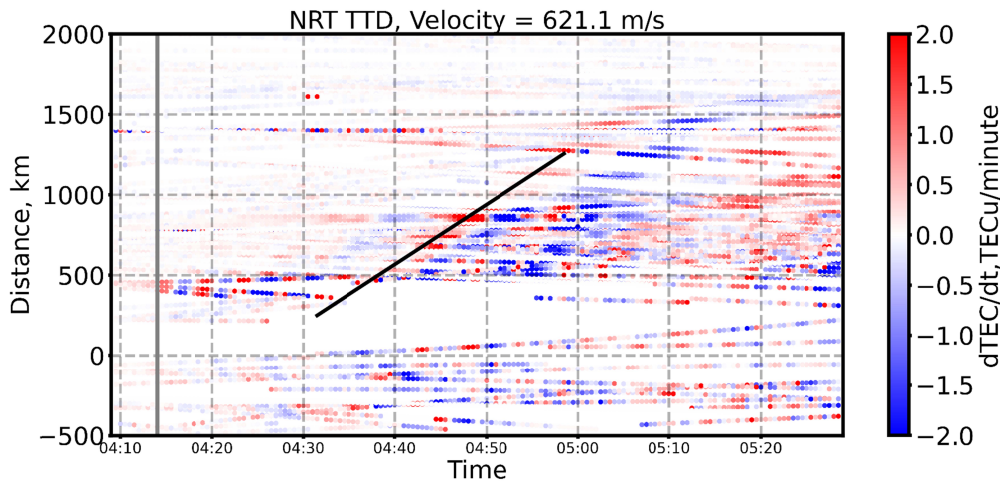
369
 370
 371
 372 **Figure 2. a)** The Hunga Tonga-Hunga Ha’apai volcano (red star, 175.382W; 20.53S) and GNSS
 373 receivers network used in this work. The receivers that are both sources of 30 sec and 1 sec
 374 cadence data: “CKIS”, “FAA1”, “FTNA”, “LAUT”, “PTVL”, “SAMO”, “SOLO”, “THTG”,
 375 “TONG”, “TOW2”, “TUVA”, “USP1”. The others provide only 30 second data; **(b-d)** The first
 376 instantaneous velocities’ field obtained by “D1-GNSS-RT”. Gray arrow shows the velocity
 377 vector of 1000 m/s. The blue arrows correspond to the instantaneous velocities’ field of co-VID;
 378 **(e-f)** the source locations obtained from the instantaneous velocities. The blue crosses correspond

379 to the source locations obtained from the instantaneous velocities' field.



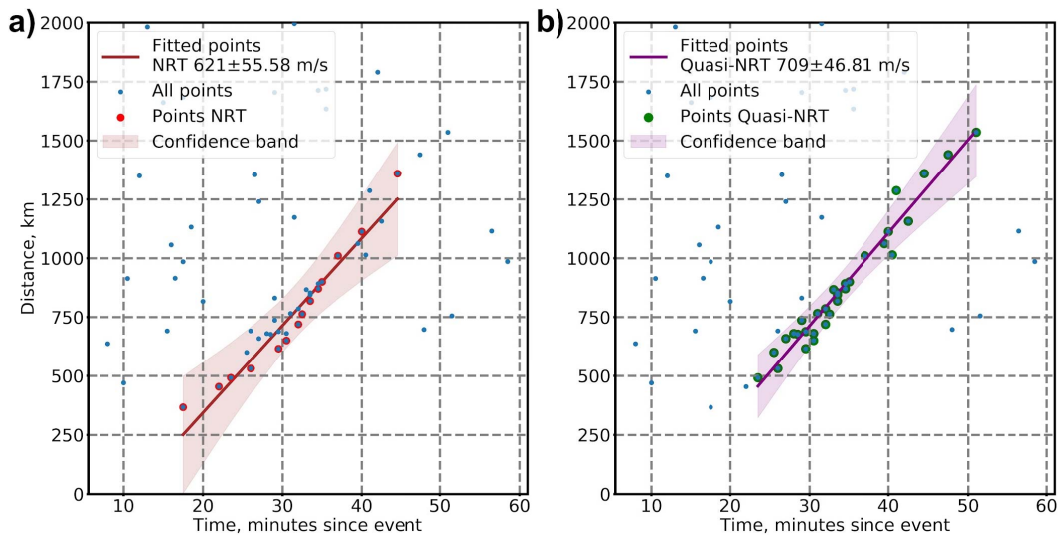
380
381
382
383
384
385

Figure 3. NRT TTD using 30-sec data and co-VID velocity (black line). Gray vertical line shows the USGS onset time. The source is located in the Hunga Tonga-Hunga Ha’apai volcano. The black line was fitted by the newly developed automatic NRT-algorithm.



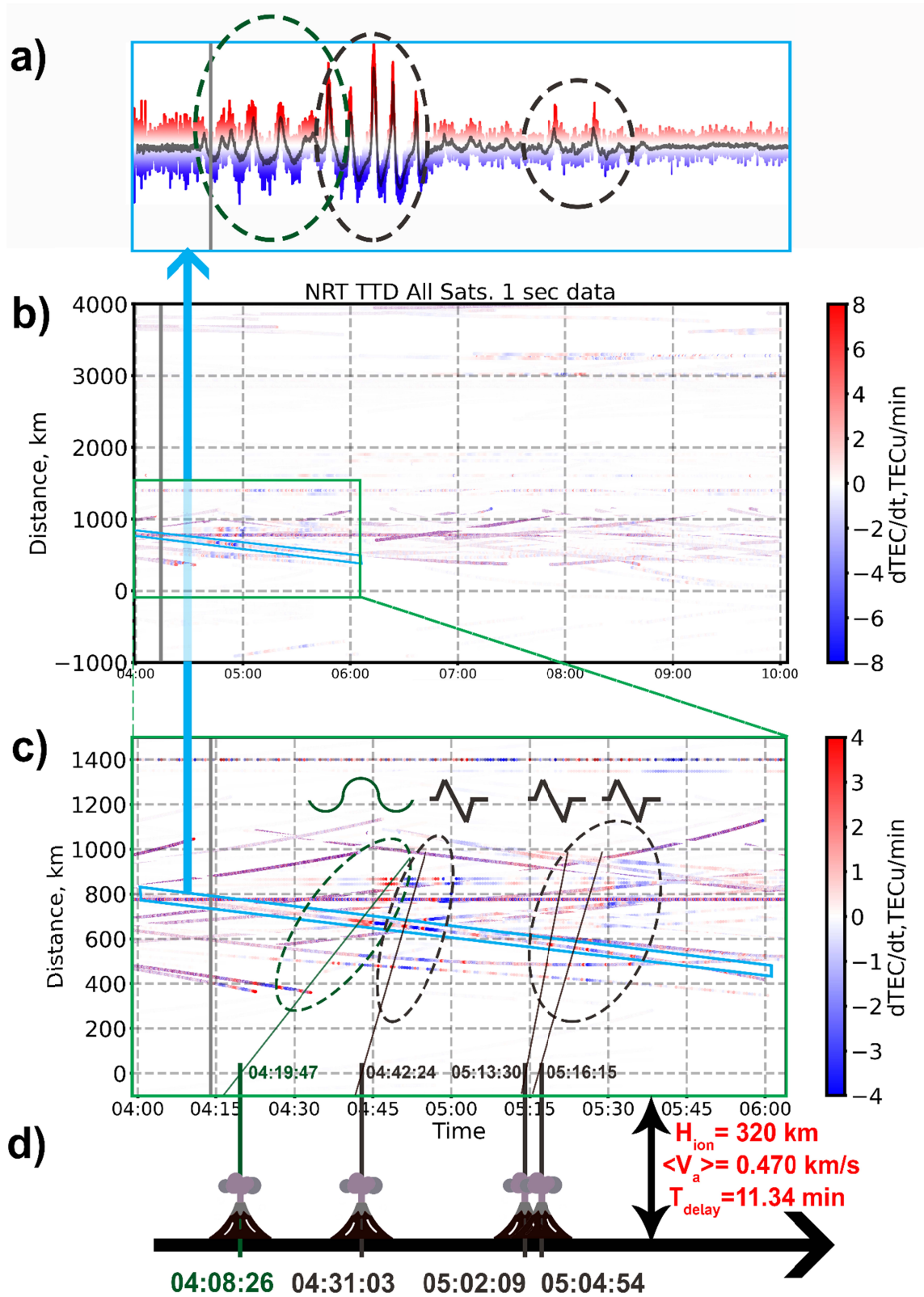
386
387
388
389
390
391
392

Figure 4. The two fitting algorithms in the TID velocity's slope: (a) the NRT - the brown line, (b) the Quasi-NRT - purple. The blue dots correspond to the first maximums of each series. The red and the green dots are used for the linear regression by the NRT and the Quasi-NRT algorithms, respectively.



393
394
395
396
397
398
399
400
401

Figure 5. (a) $dTEC/dt$ variations based on the data from receiver SAMO - satellite R21 LOS, blue-white-red curve - 1-sec data, black curve - 5 second centered smoothed data; (b, c) NRT TTD plotted using 1-sec data (b) and (c) zoom on the near-field $dTEC/dt$ response from 04:00 to 05:30 UT. Gray vertical line denotes the USGS onset time, slopes correspond to the independent signatures' velocities, proposed events highlighted in circles (in green - quasi-periodic signature, in dark brown - N-shape ones); (d) schematic representation of multi-eruption scenario and the onset time for each event



**Near-Real-Time analysis of the ionospheric response to the 15 January 2022
Hunga Tonga-Hunga Ha'apai volcanic eruption**

B. Maletckii¹, E. Astafyeva¹

¹ – Université Paris Cité, Institut de Physique du Globe de Paris (IPGP), CNRS UMR 7154, 35-39 Rue
Hélène Brion, 75013 Paris, email : maletckii@ipgp.fr

Contents of this file

Figures S1, S2, S3 and Captions
Tables S1 and Caption

Introduction

The supplementary material consists of Figures S1 - S4 and Table S1.

Figure S1 illustrates the difference between dTEC/dt parameters obtained from 30-sec and 1-sec data. 1-sec dTEC/dt signal has larger amplitudes and is more disturbed than 30-sec one.

Figure S2 shows dTEC/dt signatures generated by different sources. The biggest peak-to-peak disturbance amplitude corresponds to the 2011 Great Tohoku-Oki earthquake, however the response to the Tonga volcanic eruption has a similar amplitude, which emphasizes the unprecedented response to this eruption. Signature pick-to-pick disturbance amplitudes due to the Tonga Eruption outscore the one of the 2015 Calbuco Eruption by a factor 2.5.

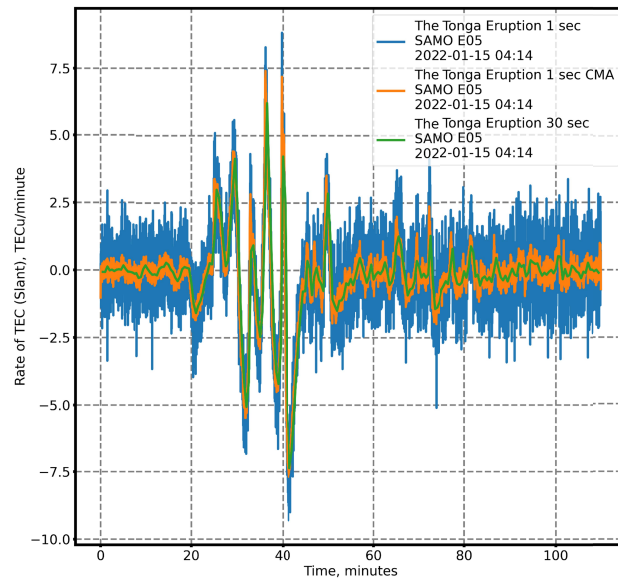
Figure S3 demonstrates the sound speed profile of the 15th of January 2022 that was used to compute weighted average velocity, and the scheme summarizing the

30 assumptions used to compute the on-ground onset time of the eruption. We use
31 this vertical velocity to estimate the on-ground onset time of the sub-eruptions.

32 Table S1 presents comparison of the eruption onset time between non-ionospheric
33 methods and our estimation based on velocities of the co-VID.

33 Figures

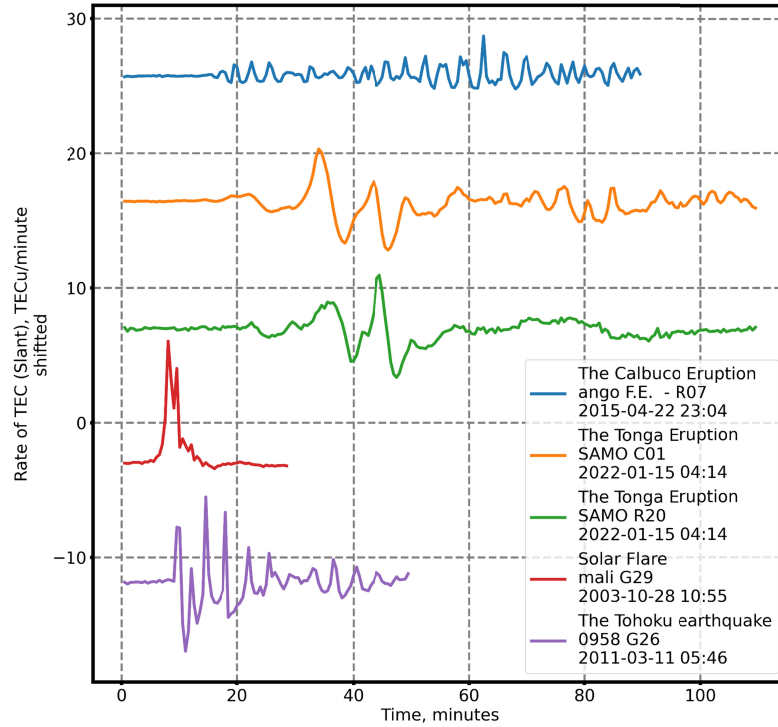
34



35

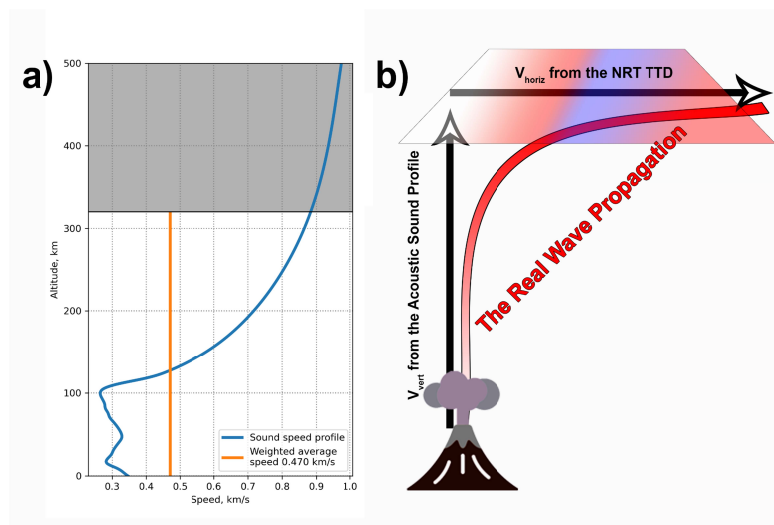
38 **Figure S1.** Comparison of $dTEC/dt$ parameters with different data cadences. The
39 blue line is 1-sec data; the orange line is 1-sec data after applying a centered moving
40 average filter (5-sec window); the green line is 30-sec data.

39



40
41
43
44
44
45

Figure S2. Comparison of $dTEC/dt$ responses generated by different sources. Time starts from the event onset.



46
47
50
51
52

Figure S3. (a) The sound speed profile for the 15 January 2022 and at the time and location of the eruption; **(b)** The scheme explaining approximations to compute on-ground onset time using vertical and horizontal components of the disturbance's

50 velocity. Horizontal velocity is obtained from “D1-GNSS-RT” and/or NRT TTD. Vertical
 51 velocity is obtained from an acoustic sound profile.
 52

Event Number	Onset USGS	Onset Poli & Shapiro (2022)	Onset Wright et. al. (2022)	Onset raw VTEC Astafyeva et al. (2022)	Onset dTEC/dt NRT TTD current study
1	04:14:45	04:16:00.07	04:28±2	04:08:43	04:08:26
2	-	-	04:36	04:20:00	04:31:03
3	-	-	05:10	04:48:30	05:02:09
4	-	-	05:51	04:55:21	05:04:54

53
 54 **Table S1:** Time onsets (UT) of 4 main HTHH volcano eruptions as estimated from on-
 55 ground techniques (USGS - column 2; Poli & Shapiro, 2022 - column 3; Wright et. al,
 56 2022 - column 4), and from the ionosphere (by using raw VTEC (Astafyeva et al.,
 57 2022) - column 5, by using the dTEC/dt NRT TTD - column 6)
 58